Measurements of Maximum Surface Pressure Deficits in Modeled Atmospheric Vortices

R. L. PAULEY, C. R. CHURCH[1] AND J. T. SNOW

Department of Geosciences, Purdue University, West Lafayette, IN 47907

(Manuscript received 13 July 1981, in final form 26 October 1981)

ABSTRACT

Time-dependent features of the wall static pressure field beneath vortices modeled in a Ward-type vortex simulator have been investigated with emphasis on measurements of maximum surface pressure deficit. A pressure-measuring system was devised for this purpose which is capable of resolving important transient features of the surface pressure field in an essentially undistorted form, and measurement techniques were employed which reduced the influence of vortex wander. Measurements of maximum surface pressure deficits and their dependence on flow rate and geometry are presented, as well as a detailed study of the magnitudes of the maximum surface pressure deficits as a function of swirl ratio. Also presented are surface pressure distributions in individual subsidiary vortices in a multiple vortex flow.

The greatest deficit pressures are found to be associated with the penetration of the vortex breakdown to the surface. The magnitude of the surface pressure deficit is closely related to the square of the mean vertical velocity of the upflow and also is dependent on swirl ratio. The pressure deficits in the subsidiary vortices presented are variable but range up to three times that found at the center of the "parent" vortex.

1. Introduction

Recent research by the investigators has focused on laboratory simulation and measurement as a means of examining in detail the dynamic features associated with tornado-like vortices and evaluating the various factors which determine vortex intensities. Experiments have been performed using a vortex generator after the design of Ward (1972). For a description of the apparatus and a discussion of the similarity criteria which apply, the reader is referred to Church *et al.* (1979). The key similarity parameters are the swirl ratio $S = r_0\Gamma/2Qh$, the radial Reynolds number $\mathrm{Re}_r = Q/2\pi\nu$, and the aspect ratio $a = h/r_0$, where Q is the volume flow rate per unit axial length, Γ is the circulation at the periphery of the convergence zone, ν is the kinematic viscosity, and h and r_0 are the height and radius of the convergence zone, respectively. The present paper provides new experimental measurements of surface pressures beneath concentrated vortices. The basis for these experiments can be found in two previous studies, Baker and Church (1979) and Snow *et al.* (1980).

In the former study, the time-averaged maximum velocity in the vortex (above the boundary layer) was measured as a function of swirl ratio at different radial Reynolds numbers. These measurements encompassed both single-celled vortices (with radial inflow and axial upflow everywhere) and two-celled vortices (with radial outflow and axial downflow near the axis, and radial inflow and axial upflow away from the axis). It was found that in the single-celled vortices, which formed at low swirl ratio, the maximum velocity increased rapidly with increasing swirl ratio. In the two-celled vortices, which formed at higher swirl ratios, only small variations in maximum velocity were observed over a wide range of swirl ratio. It also was found that when the mean vertical velocity in the updraft region was used as a scaling parameter, all the velocity data could be collapsed into a single curve. One might expect the maximum pressure deficits in vortices to vary in a similar manner to the maximum velocities and to scale correspondingly, but this expectation needs to be tested empirically.

In the study by Snow *et al.* (1980), an investigation of surface pressure fields beneath vortex flows was performed for a variety of flow conditions. Radial profiles of the time-averaged wall static pressure reflected the development of an intense single-celled vortical core and its evolution into a broader two-celled structure as the swirl ratio was systematically increased. The maximum pressure deficit, which was located at the vortex center in single-celled vortices, moved off-center in the two-celled vortices. Single-celled vortices contained larger radial pressure gradients than two-celled vortices, and the pressure deficits in single-celled vortices exhibited stronger dependence on swirl ratio than the deficits in two-celled vortices. Since the techniques employed in that study

[1] Present affiliation, Department of Aeronautics, Miami University, Oxford, OH 45056.

0022-4928/82/020369-09$06.25

involved substantial filtering, the data presented only the most persistent features of the static pressure field, and any transients were averaged out.

Previous investigations by Ward (1972) and Church *et al.* (1977) had shown, through flow visualization, that the vortex core can contain important time-dependent dynamic features, such as multiple subsidiary vortices. The partition of energy between the subsidiary vortices and other regions of the parent vortex is of particular significance in assessing the impact of tornadic flows on surface structures, and therefore the transient features of the flow field need to be investigated. It also is important that the magnitudes of the pressure deficits be measured precisely. Vortex wander presents an experimental difficulty here, particularly for single-celled vortices, in that time-averaging of measured pressure at each station results in broader pressure wells and smaller pressure deficits than those which actually exist. It is therefore desirable to examine the pressure field of simulated vortices with sensors having fast time response, in order to determine instantaneous values of maximum pressure deficit at various radial locations.

This paper presents the results of three experiments which address the above points. Instrumentation techniques were developed which enabled transient pressure perturbations to be reproduced with a high degree of fidelity. One experiment was conducted to determine the dependence of the maximum surface pressure deficits on the background flow conditions, in an attempt to discover the appropriate scaling parameters for pressure. In a second experiment, the maximum surface pressure deficit was measured as a function of swirl ratio for a fixed geometry and different values of Reynolds number. In a third experiment, a system of three pressure transducers was used to obtain simultaneous pressure recordings at three closely spaced radii in a vortex core containing subsidiary vortices. Transformation of these data provided distributions of surface pressure inside and surrounding the subsidiary vortices. Details pertaining to the operation of the modeling apparatus and pressure sensors have been presented in detail in the two articles previously mentioned, and will not be discussed further here. There are, however, some novel features concerning the adaptation and adjustment of sensors for measuring transient pressures which will be mentioned before the experimental results are presented and discussed.

2. Measurement procedures

In order to resolve important transient features of the pressure field in an essentially undistorted form, attention was paid to establishing optimum dynamic response of the pressure-measuring system. As in the experiments of Snow *et al.* (1980), pressures were measured using variable reluctance differential pressure transducers connected to static ports via lengths of tubing. Such an arrangement exhibits approximate second-order dynamic response, in which the degree of damping must be adjusted to avoid amplitude overshoots which occur in an underdamped mode, or sluggish response which is characteristic of overdamping.

To evaluate the dynamic response of the pressure-measuring system, harmonic pressure signals from an acoustic driver were applied to the static port of the transducer and monitored using a condenser-type microphone system. The microphone provided a feedback mechanism so that the rms amplitude of the pressure signal at the port could be kept constant for all frequencies. Different damping conditions could be established by varying the length and diameter of the tube connecting the port to the transducers. The damping ratios and undamped natural frequencies were estimated by fitting the data to the frequency response curves for ideal second-order oscillators. A damping ratio of $D \approx 0.64$ gives optimum frequency, transient and phase response, so each of three transducers was adjusted by trial and error to ensure that $D = 0.64 \pm 0.05$, with uncertainties due to experimental error and non-ideal response. With this degree of damping, the corner (-3 dB) frequencies of the three transducers tested were close to 20 Hz. A final check was made with the transducers installed in the vortex chamber, where they were simultaneously subjected to step-like pulses from a loudspeaker driven by a low-frequency square wave. This resulted in remarkably well-matched traces, with rise times of $\sim$26 ms. These rise times proved to be much shorter than those normally encountered in multiple vortex pressure perturbations.

Depending on the experiment being performed, pressures were measured using a single-port pressure probe, in the manner of Snow *et al.* (1980), or a triple-port probe with static ports spaced radially 2 cm apart, each port being connected to a separate transducer. The three-port system was especially developed for measurements in multiple vortices for the following reasons: 1) to reduce the uncertainty in vortex location and so help identify the occurrence of nearly diametric traversals of the central port by orbiting subsidiary vortices and 2) to make simultaneous measurements at different radial positions in order to reconstruct a portion of the pressure field associated with multiple-vortex systems. Because of dynamic response requirements, the pressure deficits were measured with respect to the ambient pressure beneath the experimental chamber rather than the surface pressure at large radius as in Snow *et al.* (1980). The pressure measurements were monitored on an oscilloscope having triple-trace storage capability, with a recording oscillograph being used to provide a hard copy of the data. The experimental

techniques required to measure radial Reynolds numbers and swirl ratios were similar to those discussed in Church *et al.* (1979).

3. Dependence of maximum surface pressure deficit on radial Reynolds number and aspect ratio

The dependence of the central pressure deficit on *swirl ratio* S was presented by Snow *et al.* (1980) in their Fig. 9. They found that the greatest central pressure deficit occurred near $S = 0.4$, which ". . . corresponded to the onset of turbulence within the core coincident with the penetration of a vortex breakdown to surface." The first objective of the current study was to determine the dependence of this maximum central pressure deficit on flow rate and flow geometry (characterized by the radial Reynolds number Re_r and the aspect ratio a, respectively).

The experimental procedure adopted was to fix the flow geometry and then vary the flow rate; for each Re_r at which a measurement was made, the swirl ratio was adjusted until the pressure drop was maximized. The position of the pressure tap was adjusted to the mean position of the vortex center, usually within <1 cm of the geometric center of the chamber. The transducer output was monitored on an oscilloscope until the pressure deficit was maximized and two or three representative extrema were observed.

Flow visualization with kerosene fog confirmed that the greatest central-pressure deficits measured were coincident with the penetration of the vortex breakdown, or laminar-to-turbulent transition, to the surface. Thus, the minimum central pressures were found to be associated with the same dynamic feature in the vortex flow for all Re_r and a. It should be emphasized that the swirl ratio at which the vortex breakdown reaches surface is not constant for all Re_r. Because of dissipation in the boundary layer, more swirl must be put in at low Re_r to achieve a given vortex transition (see Church *et al.*, 1979). However, at higher Re_r the transition swirl ratio for the laminar-to-turbulent transition at surface approaches a constant value of $S \approx 0.3$.

Measurements of maximum central pressure deficit were made for five different flow geometries and for several radial Reynolds numbers in the range $\mathrm{Re}_r = 2 \times 10^4 - 5 \times 10^4$. The measured pressure deficits increased markedly as the updraft radius was decreased and the aspect ratio increased, forcing stronger convergence. The pressure drops were found to be approximately proportional to the square of the radial Reynolds number. Since Re_r is proportional to the volume flow rate, this relationship suggested a nondimensionalization with respect to a function of a through-flow velocity. Nondimensionalization with respect to the mean vertical velocity at the updraft hole gave the best results i.e.,

$$\Delta p^* \equiv \Delta p_{\max}/\rho \bar{w}_0^2, \qquad (1)$$

where $\Delta p_{\max}$ is the maximum pressure deficit, $\bar{w}_0$ is the mean vertical velocity at the updraft hole, and ρ is the air density. The nondimensionalized data are presented in Fig. 1. While the dimensional data varied over a range of two orders of magnitude, the dimensionless data tend to fall within the narrow range $\Delta p^* = 40 \pm 8$, particularly at large Re_r. There is a trend to smaller values for $\mathrm{Re}_r < 3 \times 10^4$, but this nondimensionalization still strongly suggests that $\rho \bar{w}_0^2$ determines the magnitude of the maximum pressure deficit that can be achieved for different flow rates and geometries. Nondimensionalization with respect to a characteristic radial velocity is much less successful in collapsing the data. The data presented in the next section further suggest that the mean updraft velocity and surface-pressure minimum are closely related for almost all vortex morphologies investigated.

The effect of surface roughness on the vortex pressure deficit was investigated briefly. The experimental procedure was repeated after covering the floor of the vortex chamber with a carpet of 2.5 cm thick shag, a surface similar to that used in a study by Leslie (1977). Leslie had found that vortex-transition swirl ratios were higher over a rough surface, and likewise in this experiment more swirl was required to drive the vortex breakdown to surface and so maximize the pressure deficit. The effect of the roughened surface was to reduce the magnitude of the maximum surface pressure deficit by 50–70%; this reduction was confirmed for several Reynolds numbers and flow geometries.

4. Dependence of maximum surface pressure deficit on swirl ratio

The swirl ratio is the most important of the similarity parameters in determining the characteristic properties and morphology of modeled vortices. Therefore, it is important to determine the dependence of the surface pressure deficit on S; and because of the presence of subsidiary vortices in high swirl ratio flows it also is important to be prepared to measure the maximum pressure deficit at whatever radial position it occurs.

This was accomplished by fixing the flow rate and geometry and varying the swirl ratio by changing the speed of the rotating screen; the radial location of the pressure tap was then varied for each value of S until the pressure deficit was maximized. The outputs of the pressure transducers were monitored on an oscillosope until two or three representative extrema were observed. The signal was then filtered electronically to determine the time-mean pressure deficit at the radius at which the maximum deficit was observed. Flow visualization was used to determine the vortex morphology and transitions as a

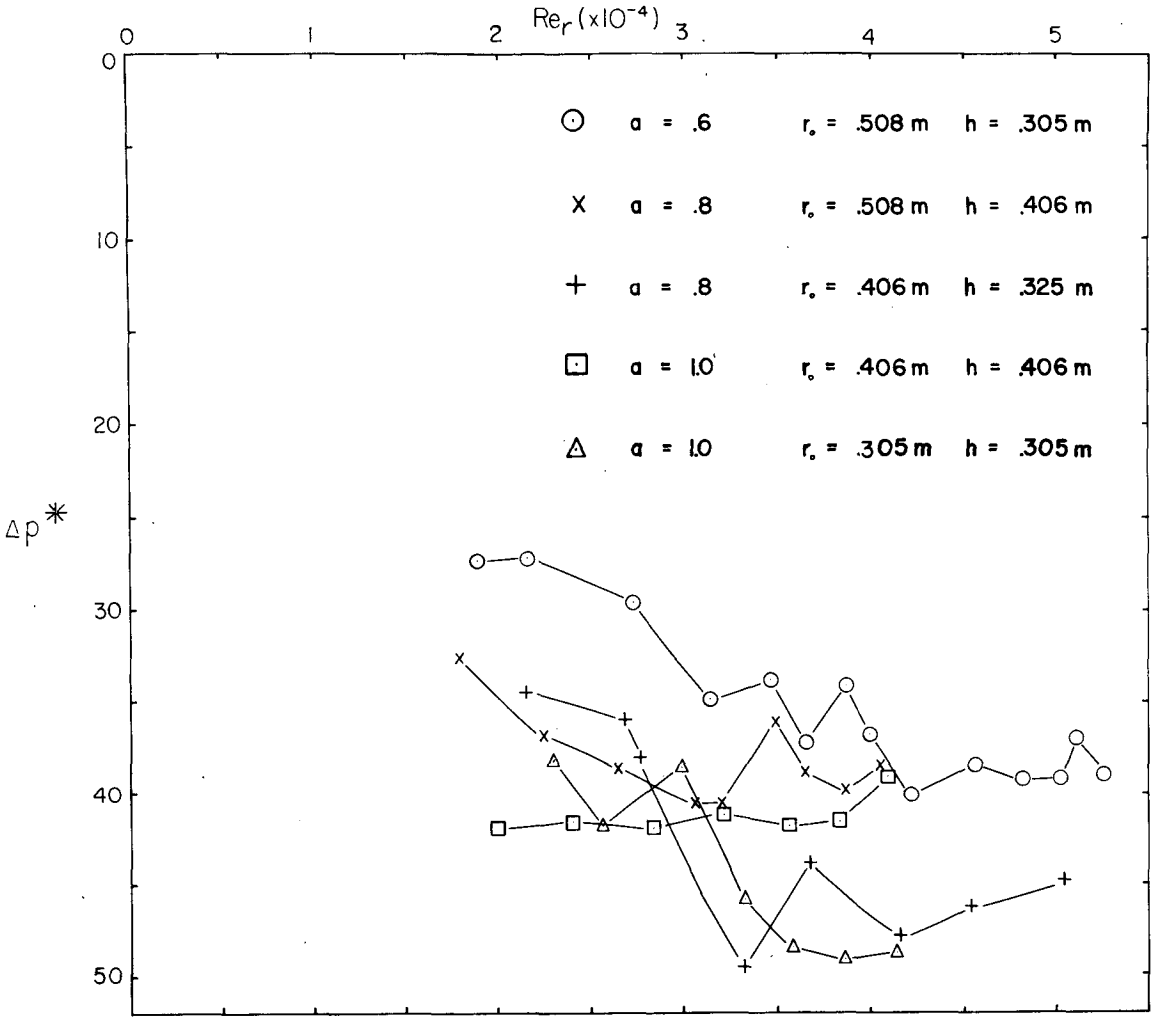

FIG. 1. Nondimensional maximum central pressure deficit at surface versus radial Reynolds number for five different flow geometries. For each point the pressure deficit was maximized by varying S.

function of swirl ratio. Transitions are defined as the change of vortex morphology at the surface.

Fig. 2 shows the maximum surface pressure deficit as a function of swirl ratio for $\mathrm{Re}_r = 2.90 \times 10^4$ and $a = 0.6$, with the pressure again nondimensionalized with $\rho \bar{w}_0^2$. The maximum pressure deficits were observed at or very near the vortex center (i.e., $r = 0$) for swirl ratios up to $S \approx 0.85$, the swirl ratio for transition from a single turbulent vortex to a pair of subsidiary vortices. After this transition, the pressure minima were associated with the subsidiary vortices and were located at ever increasing radius as the swirl ratio (and number of subsidiary vortices) was increased. At a swirl ratio of $S = 3.5$, for example, the mean position of the pressure minima had increased to a radius of 24 cm or about half of the radius of the updraft.

For single-vortex flows, Fig. 2 qualitatively resembles the plot of *central* pressure deficit versus swirl ratio in Fig. 9 of Snow *et al.* (1980); not surprisingly, significant differences emerge for the multiple-vortex flows. The behavior of the maximum pressure deficit is outlined below:

1) As the swirl ratio was increased from zero, the maximum pressure deficit increased up to $S \approx 0.20$. At these low swirl ratios ($S < 0.20$) the inflow separates at large radius and the single-celled vortex core aloft does not extend persistently to the surface.

2) At $0.20 < S < 0.25$, the maximum pressure deficit decreased sharply. Flow visualization suggests that this decrease in pressure deficit coincides with the transition from a separated to a non-separated surface boundary layer.

3) Beyond $S \approx 0.25$, the maximum pressure deficit increased precipitously as the laminar vortex core at the surface intensified and the vortex breakdown region moved upstream toward the surface. The

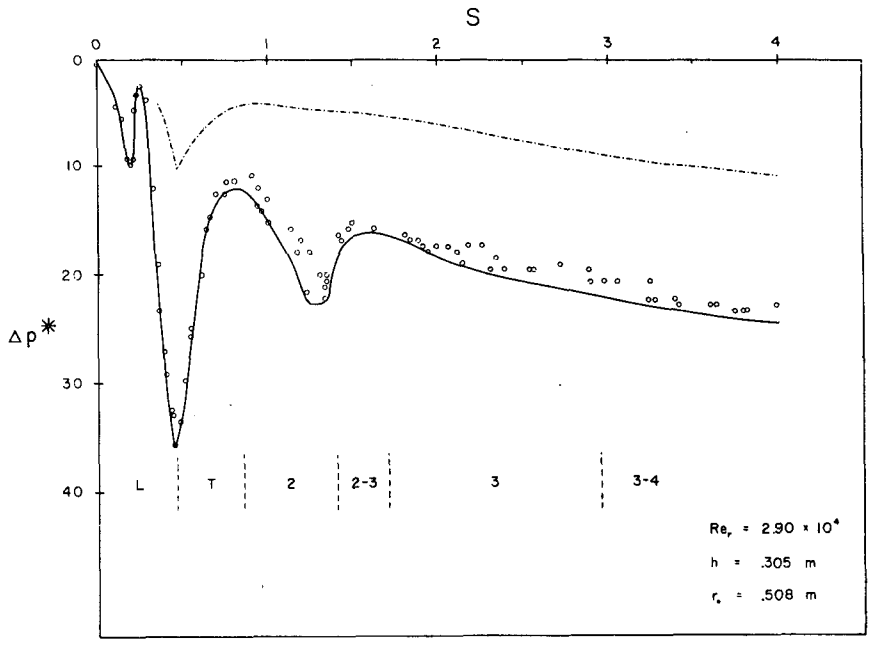

FIG. 2. Nondimensional maximum surface pressure deficit versus swirl ratio for $a = 0.6$ and $Re_r = 2.90 \times 10^4$. The plotted points represent the maximum deficits observed, with the solid curve serving as an envelope for the extrema. The vortex morphologies and transitions are indicated by the letters and numbers below the data: L (single laminar vortex), T (single turbulent), 2 (two subsidiary vortices), 2–3 (two-to-three vortex transition), etc. The dashed curve represents the time-mean pressure deficit at the radius at which the maximum deficit was observed.

greatest pressure deficit was achieved at $S \approx 0.45$ as the vortex breakdown penetrated to the surface.

4) After the transition to a turbulent vortex, further increases in swirl ratio resulted in a rapid expansion of the core radius and a decrease in the maximum pressure deficit. Flow visualization suggests that this flow regime is characterized by a two-celled structure aloft with weak central downflow.

5) As the swirl ratio was increased toward $S \approx 0.85$ a pair of subsidiary vortices developed aloft and subsequently penetrated to the surface. At this point ($S \approx 0.85$) the minimum pressure in the vortex was associated with the orbiting subsidiary vortices and was no longer located at the center of the parent vortex. The maximum pressure deficits in the subsidiary vortices then increased as the swirl ratio was increased toward $S \approx 1.40$.

6) At a swirl ratio of $S \approx 1.40$ the maximum pressure deficits realized in the subsidiary vortices decreased abruptly. This decrease occurred very near the beginning of the two-to-three vortex transition: an unsteady flow regime in which no subsidiary vortex may be evident in the visualized flow but in which two or three vortices are usually indicated by the pressure field.

7) Beyond $S \approx 1.60$ the maximum pressure deficits increased slowly and apparently monotonically with increasing swirl through the three vortex regime and the three-to-four vortex transition, but the pressure drops in the multiple vortex systems never approached those attained near the laminar-to-turbulent single vortex transition. At these high swirl ratios the two-celled circulation was fully developed with central downflow penetrating to the surface.

Two points should be made concerning the time-mean measurements of deficit pressure at the radius at which the maximum deficit was observed (the dashed curve in Fig. 2). First, for the single-vortex regime the true maximum pressure deficit was three to four times that of the time-mean value influenced by vortex wander, indicative of the strong radial pressure gradients near the core and perhaps some significant temporal fluctuations as well. Second, for the multiple-vortex regimes the time-mean value reflects a combination of the subsidiary vortex pressure drops and the depth of the "parent vortex pressure well," i.e., the pressure deficit near the center of the parent vortex and in between subsidiary vortices. Once the transition to a multiple-vortex flow has occurred, the parent pressure well deepens very little (see Fig. 9 of Snow *et al.*, 1980); the modest increase in the time-mean deficit at high swirl ratio in Fig. 2 is due largely to the increased contribution of subsidiary vortices.

Fig. 3 shows Δp^* versus S for $Re_r = 4.14 \times 10^4$ and $a = 0.6$. The plot is quite similar to that of Fig. 2. Common features include 1) an abrupt decrease

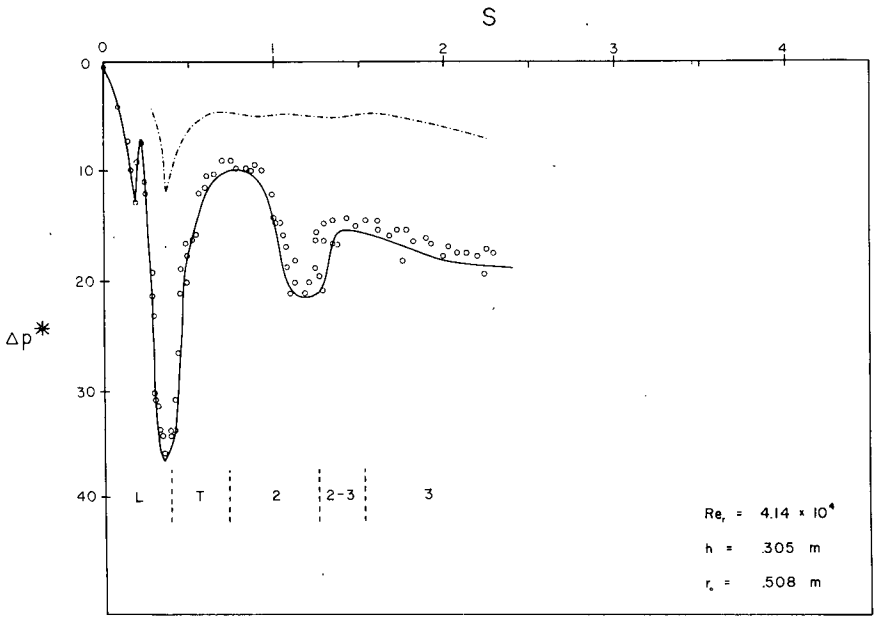

FIG. 3. As in Fig. 2 except $Re_r = 4.14 \times 10^4$.

in the pressure deficit at low swirl ratio which flow visualization indicated was coincident with the transition from a separated to a non-separated surface boundary layer ($S \approx 0.2$); 2) a maximum in the pressure deficit associated with the penetration of the laminar-to-turbulent vortex transition to surface ($S \approx 0.4$); and 3) a secondary pressure deficit maximum in the multiple-vortex flow regime ($S \approx 1.2$). The recurrence of these common features also was observed in a third set of measurements (not shown) made at $Re_r = 2.07 \times 10^4$ and $a = 0.6$.

Aside from the previously described Re_r dependence of the transition swirl ratios, perhaps the most significant difference between the three Reynolds number cases is the position and relative magnitude of the secondary pressure deficit maximum in the multiple-vortex flow regime. At higher Re_r this feature is shifted toward the two-to-three vortex transition and becomes more pronounced. Flow visualization indicated that the greatest multiple-vortex pressure deficits were associated with transient "spin-ups" of individual subsidiary vortices and momentary decreases in their core radius. From this we infer that the secondary pressure deficit maximum occurred when flow conditions favored the greatest concentration of vorticity in the fewest subsidiary vortices. The reason for the variation of this feature with Reynolds number, however, is not clear.

One final important point to note is that the scaling of the pressure deficits to the mean updraft velocity is not confined to the special case of the laminar-to-turbulent transition considered in the previous section. The data further suggest the following general relation (for a given surface roughness)

$$\Delta p_{max} = K(S, Re_r)\rho\bar{w}_0^2, \quad (2)$$

where the proportionality factor K is a complicated function of the vortex morphology as indicated by Figs. 2 and 3. Even the time-mean pressure deficits scale quite well to $\rho\bar{w}_0^2$. The relation in Eq. (2) fails only for low Re_r ($<2 \times 10^4$) or very small S (<0.3).

5. Surface pressure distributions in subsidiary vortices

The preceding sections have examined the swirl ratio, Reynolds number, and aspect ratio dependence of the maximum surface pressure deficits in multiple-vortex flows but have given no indication as to the actual pressure distribution in an individual subsidiary vortex. In this section, surface pressure distributions in individual subsidiary vortices are presented in plan form for a select set of flow conditions.

The previously described triple-port probe and three pressure transducers were employed for these subsidiary vortex measurements. The aspect ratio and radial Reynolds number chosen were those at which the most pressure data had previously been gathered, $a = 0.6$ and $Re_r = 2.9 \times 10^4$. The swirl ratio chosen, $S = 2.45$, corresponded to a pattern of three subsidiary vortices orbiting at a mean radius of 19 cm with a period of $\sim$1.0 s. Also, the surface pressure deficits for these flow conditions were large enough to maintain a favorable signal-to-noise ratio.

The triple-port probe was positioned on the lower surface of the chamber with the ports located at radii of 17, 19 and 21 cm (some measurements were made at 18, 20 and 22 cm). Employing Taylor's hypothesis,

which supposes that a record of some quantity (in this case pressure deficit) is due to a simple translation of a spatial flow pattern, the temporal record from the oscillograph was transformed into a spatial representation of the pressure field. The angular velocity and orbital radius of the subsidiary vortices about the parent vortex centerline were assumed to be constant for the purpose of the transformation, so that each trace was taken to represent the pressure deficit along a constant radius in the parent vortex. Using all three traces, limited-area plan form pressure fields for individual subsidiary vortices such as those shown in Fig. 4 were synthesized. Fig. 5 represents a case in which three successive subsidiary vortices passed close to the array of pressure ports and an annular-shaped region of the pressure field was reconstructed.

Even though every effort was made to select flow conditions (S, Re_r, a) that produced a steady pattern of vortices, the subsidiary vortices observed displayed considerable diversity both quantitatively and qualitatively. For a sampling of 15 subsidiary vortices (not all shown), the total pressure deficits ranged from 12 to 24 Pa. Pressure deficits measured near the center of the parent vortex and the deficits in between subsidiary vortices were in the range 7–9 Pa for the flow conditions specified, so the subsidiary vortices contained pressure drops that were two to three times greater than the "parent pressure well." The subsidiary vortex pressure fields also displayed

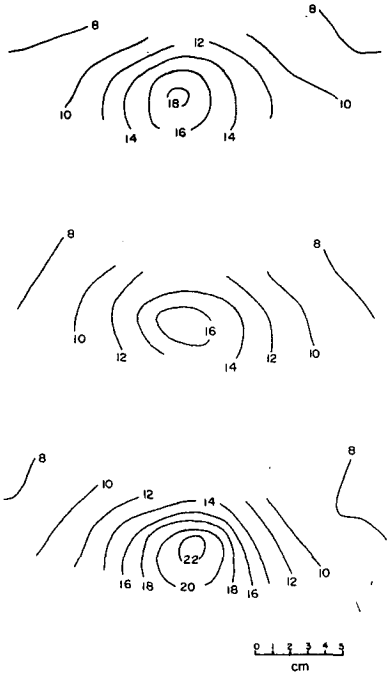

FIG. 4. Surface deficit pressure fields over a limited area for three individual subsidiary vortices. S = 2.45, $\mathrm{Re}_r = 2.90 \times 10^4$, a = 0.6. Units of deficit pressure are Pascals.

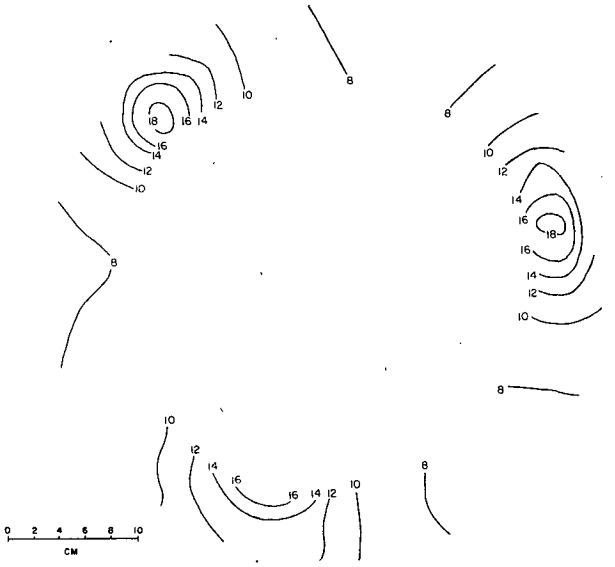

FIG. 5. Surface deficit pressure fields over a limited area for three successive subsidiary vortices. S = 2.45, $\mathrm{Re}_r = 2.90 \times 10^4$, a = 0.6. Units of deficit pressure are Pascals.

a variety of asymmetries, probably not a surprising result for orbiting vortices. One frequently observed feature, for example, was a slightly stronger pressure gradient on the side of the subsidiary vortex closer to the center of the parent vortex, qualitatively similar to the idealized case of a circular array of potential vortices. Certain asymmetries in the reconstructed pressure distributions might also result from the failure of the assumptions used in the temporal to spatial transformation.

Individual raw pressure traces from those events representing nearly diametric subsidiary vortex traversals also are useful. For example, such a trace may be used to estimate the local subsidiary vortex core radius, taken as the point of maximum rotational velocity about the subsidiary vortex, which should approximately correspond to the inflection point in the pressure trace. Although the precise location of the inflection point is often difficult to determine, traces indicate core radii of 2–3 cm for the stronger subsidiary vortices observed, corresponding to 10–15% of the parent vortex core radius of 20 cm.

6. Discussion and conclusions

The two most significant findings of this investigation are 1) the scaling of the surface pressure deficits to $\rho\bar{w}_0^2$, and 2) the fact that the greatest deficit pressures are associated with the single-celled vortex just upstream of the breakdown and not with the subsidiary vortices in a multiple-vortex system at the same $\rho\bar{w}_0^2$. While the second finding may be a little surprising, neither of these results were totally unexpected.

The quantity $\rho\bar{w}_0^2$ is taken to characterize the axial momentum flux (or alternatively, the *flow force*, following the definition of Morton, 1969) of the gross upflow in which the vortex is embedded. This quantity plays an important role in the dynamics of any vortex formed in the upflow. At first glance, the pressure field beneath a concentrated columnar vortex is determined largely by the azimuthal velocity field through the radial momentum equation. However, the azimuthal and axial flows in the vortex core are coupled through the pressure field, and the core perturbation pressures scale to both characteristic axial and azimuthal core velocities [see the analysis of Morton (1966) for narrow columnar vortices]. Further, the strength of the axial flow in the vortex core for a given swirl ratio should be related to the magnitude of the gross axial flow force characterized by $\rho\bar{w}_0^2$. So it is not surprising that the surface pressure deficits scale well to $\rho\bar{w}_0^2$. In this general connection it should be noted that in the laboratory the background circulation and through-flow (or S and Re_r) can be varied independently; such decoupling of the gross flow features is probably not the case in the atmosphere, and the nature of the coupling between gross through-flow and circulation may be crucial in determining the strength and character of geophysical vortices (see Lewellen, 1976).

The occurrence of the greatest surface pressure deficits as the vortex breakdown reaches surface may be viewed as follows. First, the breakdown represents not only a transition to turbulent flow, but also a corresponding abrupt increase in the core radius (for a review of the vortex breakdown phenomenon, see Leibovich, 1978). When the vortex breakdown is driven near the surface by increasing swirl, the tangential velocities in the small-radius laminar core just below the breakdown are maximized via conservation of angular momentum. So a corresponding maximum in the pressure deficit is expected. Moreover, in single-celled vortices there is a vertical pressure gradient in the turning region at the base of the vortex core where the flow is accelerated upward. In laboratory vortex measurements, Ying and Chang (1970) found that the vertical pressure gradients in this region were quite sharp, with the lowest pressure occurring a small distance above the surface. Work in progress at Purdue University suggests that the swirling velocities and pressure deficit *aloft* are maximized as the vortex breakdown reaches the top of the surface boundary layer. As the breakdown subsequently penetrates through the boundary layer, the *surface* pressure deficit is maximized as more and more of the pressure deficit aloft is realized at the surface. Once the breakdown has penetrated all the way to the surface, the pressure deficits decrease with increasing swirl as the core radius expands in the single turbulent vortex regime. The numerical tornado modeling results of Smith and Leslie (1979) also show that increasing the imposed circulation can lead to decreased tangential velocities (and presumably decreased deficit pressures) in a vortex core due to an increase in the core radius. That the maximum pressure deficit associated with the vortex breakdown should be greater than the deficits in a *multiple* vortex system is less obvious. The greatly increased size of the core at large swirl ratio evidently more than offsets the effects of the increased input of circulation, even when subsidiary vortices provide small localized centers of convergence at the outer edge of the core.

The third important result of this study was the measurement of surface pressures in subsidiary vortices. While subsidiary vortices did not contain pressure drops as great as those associated with the vortex breakdown, they *were* found to contain pressure drops two to three times greater than the pressure well of the parent vortex in which they were embedded. The subsidiary vortex pressure deficits also were significantly greater than the pressure deficit in the single turbulent vortex just prior to its transition to a multiple vortex system.

There is probably no unique relationship between the surface pressure deficit and the maximum vortex velocity, but rather this relation depends on swirl ratio or vortex morphology (Leslie, 1979). However, there is good evidence that even if the surface pressure deficit does not uniquely quantify the maximum vortex velocity, it is still a reliable qualitative indicator of vortex strength. As noted in the introduction, the scaling of the mean maximum vortex velocity to $\bar{w}_0$ was illustrated in the study by Baker and Church (see their Fig. 3). With regard to swirl ratio dependence, their data show a rapid increase in $|V_{max}|/\bar{w}_0$ versus S at low swirl ratio ($S < 0.4$), and two slight peaks in the maximum velocity at $S \approx 0.5$ and $S \approx 1.3$. They associated these two peaks with the laminar-to-turbulent transition and a well-developed double vortex structure, respectively. At higher swirl ratios the maximum velocity increases only modestly. Thus, there is good qualitative agreement between our measurements of maximum pressure deficit (Figs. 2 and 3) and the time-averaged maximum vortex velocities measured by Baker and Church. Detailed time-*dependent* measurements of maximum vortex velocities as a function of swirl ratio, although experimentally difficult (Leslie, 1979), still need to be pursued in future work.

Acknowledgments. The authors wish to thank Dr. Joseph Sullivan and Mr. Glenn Baker for their cooperation and assistance in calibrating and testing the measurement system. Also, sincere thanks go to Ms. Debbie Burks for typing this manuscript. This research was sponsored by the National Science Foundation under Grants ATM 77-16955 and ATM 80-03403.

REFERENCES

Baker, G. L., and C. R. Church, 1979: Measurements of core radii and peak velocities in modeled atmospheric vortices. *J. Atmos. Sci.*, **36,** 2413–2424.

Church, C. R., J. T. Snow and E. M. Agee, 1977: Tornado vortex simulation at Purdue University. *Bull. Amer. Meteor. Soc.*, **58,** 900–908.

——, J. T. Snow, G. L. Baker and E. M. Agee, 1979: Characteristics of tornado-like vortices as a function of swirl ratio: a laboratory investigation. *J. Atmos. Sci.*, **36,** 1755–1776.

Leibovich, S., 1978: The structure of vortex breakdown. *Annual Review of Fluid Mechanics*, Vol. 10, Annual Reviews, Inc., 221–246.

Leslie, F. W., 1977: Surface roughness effects on suction vortex formation: a laboratory simulation. *J. Atmos. Sci.*, **34,** 1022–1027.

——, 1979: The dependence of maximum tangential velocity on swirl ratio in a tornado simulator. *Preprints Eleventh Conf. Severe Local Storms*, Amer. Meteor. Soc., 361–366.

Lewellen, W. S., 1976: Theoretical models of the tornado vortex. *Proc. Symp. on Tornadoes: Assessment of Knowledge and Implications for Man.* Texas Tech University, Lubbock, 107–143. [Available from the Inst. for Disaster Research, Texas Tech University].

Morton, B. R., 1966: Geophysical vortices. *Progress in Aeronautical Sciences*, Vol. 7, D. Kucheman, Ed., Pergamon Press, 143–194.

——, 1969: The strength of vortex and swirling core flows. *J. Fluid Mech.*, **38,** 315–333.

Smith, R. K., and L. M. Leslie, 1979: A numerical study of tornadogenesis in a rotating thunderstorm. *Quart. J. Roy. Meteor. Soc.*, **105,** 107–127.

Snow, J. T., C. R. Church and B. J. Barnhart, 1980: An investigation of the surface pressure fields beneath simulated tornado cyclones. *J. Atmos. Sci.*, **77,** 1013–1026.

Ward, N. B., 1972: The exploration of certain features of tornado dynamics using a laboratory model. *J. Atmos. Sci.*, **29,** 1194–1204.

Ying, S. J., and C. C. Chang, 1970: Exploratory model study of tornado-like vortex dynamics. *J. Atmos. Sci.*, **27,** 3–14.